Electronic structure of iron silicides grown on Si(100) determined by photoelectron spectroscopies

J. Alvarez, J. J. Hinarejos, E. G. Michel, G. R. Castro,* and R. Miranda
Departamento de Física de la Materia Condensada C-III, Universidad Autónoma de Madrid, E-28049 Madrid, Spain
(Received 18 July 1991; revised manuscript received 22 October 1991)

We have studied the growth of Fe on Si(100)2×1 and the formation of FeSi and β-$FeSi_2$ by solid-phase epitaxy and reactive-deposition epitaxy. The silicide films were characterized by x-ray photoelectron spectroscopy to determine their atomic stoichiometry and their characteristic plasmon loss structure. Bulk single crystals of FeSi and α-$FeSi_{2.3}$ were analogously characterized, which allowed us to establish the nature of the *in situ* grown silicide films. The electronic structure of these FeSi and β-$FeSi_2$ films were carefully studied by ultraviolet photoelectron spectroscopy, and compared with previously published theoretical calculations. A clear difference between the valence-band features of FeSi and β-$FeSi_2$ was observed, which allowed us to monitor their appearance during the growth process, and to optimize the relevant experimental parameters in order to obtain the desired phase and improve the quality of its epitaxy.

I. INTRODUCTION

The electronic structure of transition-metal silicides has been actively studied during the last few years.[1] Both the fundamental properties of these materials and their technological applications[2] justify the effort. Most of the silicides are metallic and some of them (e.g., $CoSi_2$ and $NiSi_2$) can be grown epitaxially on Si.[3,4] To achieve a detailed understanding of silicides, one must determine composition, geometry, and electronic properties under controlled conditions. This is usually done by depositing a metal film on Si substrates under ultrahigh vacuum (UHV) conditions and annealing to selected temperatures to promote the formation of the different silicides. The reaction can be followed *in situ* by a variety of experimental techniques.[5] In particular, photoelectron spectroscopies have been extensively used in the past to monitor the reaction of many metal/Si couples and to study the electronic structure of the resulting metallic silicides.[5]

Recently, much interest in *semiconducting* silicides has arisen from their possible application to integrate optoelectronic devices within the well-developed Si technology. Among the semiconducting silicides, β-$FeSi_2$ with a band gap of 0.85 eV (Refs. 6–9) has appeared as a promising candidate. In spite of an increasing number of studies devoted to the Fe/Si system,[10–27] our knowledge of the formation sequence and other properties of iron silicides is still very limited. In the Fe-Si bulk phase diagram, $FeSi_2$ exists in two crystallographic phases: α-$FeSi_2$, tetragonal[10] ($a=b=2.70$ Å, $c=5.14$ Å), metallic and stable at high temperatures (≥ 900 °C); and β-$FeSi_2$, orthorhombic[6,7] ($a=9.86$ Å, $b=7.79$ Å, $c=7.83$ Å), semiconducting,[8,9] and stable at low temperatures (≤ 900 °C). Rapid cooling during growth preserves the α phase in a metastable state at room temperature (RT). The α phase of $FeSi_2$ displays a metallic behavior with a RT resistivity of 250 $\mu\Omega$ cm. The conductivity is temperature independent, indicating a major role of defect scattering.[16,17] This phase exists in a wide range of composition, since it is intrinsically nonstoichiometric, with a content of Fe vacancies up to 13–23 %.[16,17] As grown, the β phase of $FeSi_2$ is degenerately p doped, with a carrier concentration of $\sim 10^{19}$ cm^{-3} (Refs. 19 and 20) and a low hole mobility of 1–3 $cm^2/V\,s$.[19,20] In addition to the α and β phases of $FeSi_2$, one finds other stable compounds in the Fe-Si bulk phase diagram that may appear during growth, such as Fe_3Si and FeSi. Fe_3Si is a poor metal that crystallizes in the cubic phase with $a=5.66$ Å. FeSi is a semimetal with $\rho=240$ $\mu\Omega$ cm (note that metallic Fe has $\rho=9.8$ $\mu\Omega$ cm) and has a cubic structure with $a=4.49$ Å.

It has a been proposed that the semiconducting β phase can be grown epitaxially on Si(100) with the [011] direction of silicon parallel to the [010] or [001] direction of β-$FeSi_2$,[11] and some experimental workers have studied this possibility by using solid-phase epitaxy (SPE),[12,14] reactive-deposition epitaxy (RDE),[11,13] or coevaporation.[11,15] In order to optimize the conditions of growth it is crucial to be able to identify *in situ* the Fe-Si compounds that may appear depending on the growth parameters (temperature, Fe coverage, etc.). The knowledge of their respective compositions, metallic or semiconducting character, etc., is essential to achieve the goal of epitaxial films of β-$FeSi_2$ grown on Si wafers.

In this work we set out to characterize the electronic structure of different iron silicides grown on Si(100) by SPE and RDE. We have identified the stoichiometry of the different compounds (FeSi and $FeSi_2$) by means of x-ray photoelectron spectroscopy (XPS). We have determined the density of states (DOS) of these silicides by ultraviolet photoelectron spectroscopy (UPS) and compared with calculated DOS whenever they were available. Special emphasis has been given to the determination of the metallic or semiconducting character of the various compounds. We have found that β-$FeSi_2$ films are indeed semiconducting with the Fermi level close the the valence-band edge, pinned by a high density of defects. In addition to the phases present in the bulk phase dia-

gram we have found evidence for a metallic phase probably related to the strained, fluorite $FeSi_2$ phase reported on Si(111).[28] This phase seems to be stabilized only by epitaxial growth on Si substrates. In order to have standards to compare with, we have studied also single crystals of FeSi(100) and α-$FeSi_{2.3}$(100). The results described below provide a detailed characterization of the electronic structure of epitaxial iron silicides and indicate that a high energy resolution (as obtained in UPS) is essential to decide on several important properties of the *in situ* grown films.

II. EXPERIMENTAL

The experiments were carried out in an UHV chamber (base pressure: 1×10^{-10} mbar) equipped with x-ray photoelectron spectroscopy, ultraviolet photoelectron spectroscopy, Auger-electron spectroscopy (AES), ion scattering spectroscopy (ISS), and a quadrupole gas analyzer. The FeSi(100) and α-$FeSi_{2.3}$(100) single crystals were cleaned by Ar^+ bombardment and annealing to 800 °C. This procedure provides a clean, stoichiometric surface of FeSi(100).[21] Nevertheless, depending on the detailed preparation conditions, an Fe enrichment at the surface could take place. Samples prepared analogously in a second UHV chamber equipped with low-energy electron diffraction (LEED) showed a 1×1 square pattern in the case of FeSi(100) and no LEED pattern in the case of α-$FeSi_{2.3}$(100).[15] The substrates used for the epitaxial growth were Si wafers (p type, 10^{15} cm^{-3}) oriented in the [100] direction. They were cleaned by cycles of Ar^+ sputtering and annealing to 900 °C. After some cycles no traces of contamination were observed (in particular C, O, Ni, Cu) within AES and XPS sensitivity. Similar samples analogously prepared in another UHV chamber equipped with LEED always provided sharp two-domain 2×1 patterns. Iron was evaporated from a 99.998% pure Fe wire wrapped around another resistively heated W wire. The XPS spectra were taken by using the Mg $K\alpha$ line (photon energy: 1253.6 eV) in the constant-resolution mode of the hemispherical analyzer (Leybold LHS-10, pass energy: 50 eV). The typical count rate in the Si 2p core level was 2500 counts/s above the background level. For the angle-integrated UPS spectra, the He I line (photon energy: 21.2 eV) was utilized. The pass energy was set to 5 eV in this case. The Fermi level was determined from thick metallic films. Among the various criteria that can be used to quantify the energy resolution of the electron spectrometers, we will quote in this paper the resolution as the energy range above E_F which still shows a measurable count rate above the background. With this definition, our energy resolution for a metallic Fermi edge (taken with He I) is 0.1 eV.

III. RESULTS AND DISCUSSION

A. Identification of iron silicides

When using photoelectron spectroscopies, three methods can be employed to determine the stoichiometry and identify the iron silicides: quantitative XPS, the energy values of the plasma losses, and the DOS of the valence band as given by UPS. The first method uses the formalism developed for quantitative XPS of homogeneous alloys.[29] It is based on measuring the intensity ratio of the Fe 3p and Si 2p (kinetic energy $\sim$1150 eV) core levels,[23] which can be easily converted into an atomic ratio, a useful parameter to determine the stoichiometry of the grown silicide. Assuming that the samples are homogeneous and the thickness of the grown silicide (or the bulk crystal) is larger than our sampling depth, the signals of Si [I(Si 2p)] and Fe [I(Fe 3p)] are related to the atomic density ratio X_{Fe}/X_{Si} according to the following expression:

$$\frac{X_{Fe}}{X_{Si}} = A\frac{I(\text{Fe }3p)}{I(\text{Si }2p)} \tag{1}$$

with A equal to

$$A = \frac{I_{Si}^{\infty}}{I_{Fe}^{\infty}}\frac{\lambda_{Fe}(1200)}{\lambda_{Si}(1150)}\frac{\lambda_{FeSi}(1150)}{\lambda_{FeSi}(1200)}\frac{a_{Si}^3}{a_{Fe}^3}, \tag{2}$$

where I_{Si}^{∞}, I_{Fe}^{∞}, are, respectively, the intensities of the Fe 3p and Si 2p peaks for bulk samples measured under the same conditions; $\lambda_{Fe}(1200)$, $\lambda_{Si}(1150)$ are the inelastic mean free paths (IMFP's) of Fe 3p photoelectrons in Fe and of Si 2p photoelectrons in Si. We take for these IMFP's the experimentally determined values of 10.5 and 23.0 Å, respectively (see Sec. III B). The value of 10.5 Å was measured for 1150 eV kinetic energy, but the difference with the value at 1200 eV should be very small; $\lambda_{FeSi}(1200)$ and $\lambda_{FeSi}(1150)$ are, respectively, the IMFP of photoelectrons of 1200 or 1150 eV escaping through the silicide layer; and a_{Si}^3/a_{Fe}^3 is the ratio of atomic volumes. Note that $\lambda_{FeSi}(1150)/\lambda_{FeSi}(1200)$ can be taken as equal to unity, in view of the close kinetic energies.

Tables I and II present a summary of I(Fe 3p)/I(Si 2p) ratios for measurements carried out on FeSi(100) and α-$FeSi_{2.3}$(100) single crystals as well as on thick films of epitaxial FeSi and $FeSi_2$ grown on Si(100) (see below). The values corresponding to films of FeSi and $FeSi_2$ are 0.88±0.1 and 0.46±0.05, respectively. These Fe 3p/Si 2p ratios translate into X_{Fe}/X_{Si} atomic fractions of $X=1.1\pm0.1$ and 0.6±0.1, in nice agreement with the expected ratios for FeSi and $FeSi_2$. The I(Fe 3p)/I(Si 2p) ratio for FeSi(100) lies close to the one for the film, while for α-$FeSi_{2.3}$(100) there appear two values: 0.59 for an Ar^+ sputtered sample and 0.37 for the same sample after annealing (see below). The ratio for the β-$FeSi_2$ film lies between these two values. In conclusion, it is evident that FeSi and $FeSi_2$ can easily be distinguished by XPS since they give I(Fe 3p)/I(Si 2p) ratios of $\sim$0.9 and $\sim$0.5, respectively.

TABLE I. I(Fe 3p)/I(Si 2p) intensity ratio and Fe LVV plasmon loss energy (E_p, eV) for different FeSi samples: 1, FeSi/Si(100); 2, FeSi(100). All values ±10%.

	1	2
I(Fe 3p)/I(Si 2p)	0.88	0.90
E_p	21.9	22.1

TABLE II. I(Fe $3p$)/I(Si $2p$) intensity ratio and Fe LVV plasmon loss energy (E_p, eV) for different $FeSi_2$ samples: 1, β-$FeSi_2$/Si(100); 2, β-$FeSi_2$/Si(111); 3, α-$FeSi_{2.3}$(100) (sputtered and annealed); 4, α-$FeSi_{2.3}$(100) (sputtered). All values ±10%.

	1	2	3	4
I(Fe $3p$)/I(Si $2p$)	0.46	0.42	0.37	0.59
E_p	20.7	20.8	20.8	

The characterization of the stoichiometry was completed by simultaneously measuring the x-ray excited Fe LVV Auger peak at 702.6 eV of kinetic energy. This peak displays in the case of the iron silicides a conspicuous plasmon loss,[23] whose energy depends on the density of valence electrons around the Fe atom that emits the Auger electron, and thus, on the nature of the silicide. The corresponding plasma losses were also recorded for FeSi(100) and α-$FeSi_{2.3}$(100) single crystals, and for a thick β-$FeSi_2$ layer grown on Si(111). The measured values of the energy loss appear in Tables I and II, and display also an excellent agreement with the values obtained for our silicides grown *in situ*. Thus, the plasmon energy can be used as a means of identification, since for all FeSi and $FeSi_2$ samples, the corresponding plasma loss energies are around 22.0±0.1 and 20.8±0.1 eV, respectively.

The valence-band DOS (as measured with angle-integrated UPS), can also be used to identify the various silicides. Figure 1 reproduces UPS spectra for α-$FeSi_{2.3}$(100) and FeSi(100) single crystals and thick films of β-$FeSi_2$ and FeSi grown on Si(100) (see below). The energy resolution, as defined above, is 0.1 eV, except for the FeSi(100) spectrum, which was recorded in a different spectrometer[21] with lower (0.25 eV) resolution. Both FeSi [Figs. 1(a) and 1(b)] samples are characterized by a metallic Fermi edge, an intense peak at ~0.55 below E_F and a broad, less intense, maximum at ~1.8–2.0 eV. β-$FeSi_2$ [Fig. 1(c)], on the other hand, has negligible emission at E_F (a factor 20 less than metallic FeSi), an extrapolated valence-band edge 0.1 eV below E_F, and a characteristic, well-resolved, three-peak structure. The peaks are situated at ~0.8, 1.3, and 1.6 eV below E_F and have comparable intensity at this photon energy.

In the case of the α-$FeSi_{2.3}$(100) sample, we present two spectra which correspond to a sputtered and nonannealed surface [Fig. 1(e)] and to a surface that was sputtered and annealed to 800 °C for 5 min [Fig. 1(d)]. α-$FeSi_{2.3}$(100) is metallic according to transport measurements,[16,17] and both spectra show indeed emission at the Fermi level. Apart from this, the spectra look rather different. The spectrum of the sputtered sample displays peaks at 0.5, 1.0, and 3.1 eV, while the one of the annealed sample shows three peaks very similar to those of the β phase. Except from a shift in energy by 0.15 eV towards E_F, the DOS seems to be in this case almost identical to β-$FeSi_2$. Since α-$FeSi_{2.3}$ is metastable below 900 °C, our annealing of the sample to 800 °C could favor the formation on the surface of β-$FeSi_2$ grains. Accordingly, we suggest that the spectrum of the nonannealed sample is representative of α-$FeSi_2$ while, upon annealing to 800 °C, the surface region sampled by UPS has converted into β-$FeSi_2$.

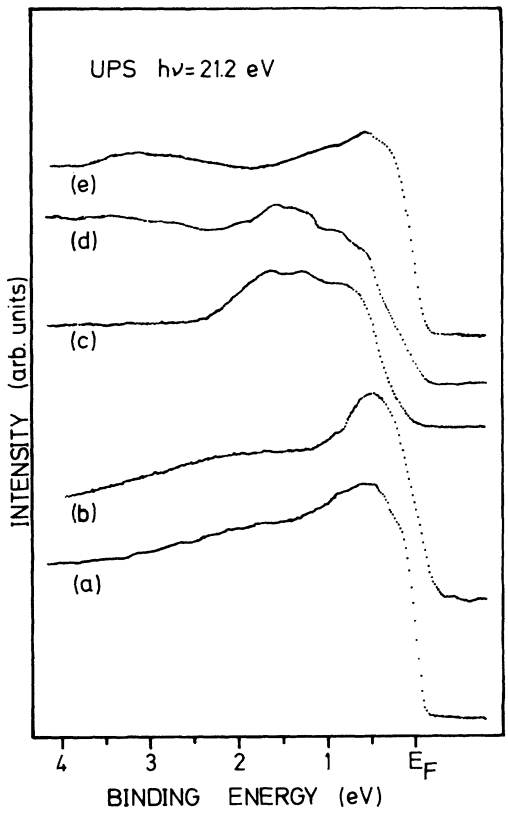

FIG. 1. Angle-integrated UPS spectra for different silicides: (a) thick FeSi layer grown *in situ* on Si(100); (b) FeSi(100) single crystal; (c) thick, β-$FeSi_2$ film grown *in situ* on Si(100); (d) α-$FeSi_{2.3}$(100) Ar^+-sputtered and annealed to 800 °C; (e) α-$FeSi_{2.3}$(100) sputtered and nonannealed. Note the similarity between spectra (a) and (b), and between spectra (c) and (d).

The electronic structure of bulk, polycrystalline iron silicides has been previously studied by photoelectron spectroscopies.[24] Thus core levels and valence-band spectra of Fe_3Si, FeSi, and α-$FeSi_2$ taken with XPS exist in the literature.[24] Unfortunately, in this work of Egert and Panzner,[24] the energy resolution (as defined above) was modest for the valence band (~0.8 eV) and, even worse, some phases could hardly be distinguished. For example, the spectra for α-$FeSi_2$ and FeSi showed identical line shapes and features, with two peaks at 0.8 and 2.0 eV below E_F. Fe_3Si displayed a different line shape, but the same two peaks. De Crescenzi *et al.*[25] reported an XPS spectrum of the valence band of a thick film of β-$FeSi_2$ grown by SPE on Si(111). Peaks were reported at 1.7 and 4 eV below E_F. The energy resolution was poor (~1.5 eV), leading to substantial emission at E_F for β-$FeSi_2$ ($\frac{2}{3}$ of the count rate observed for metallic Fe) and rising doubts on the capability of distinguishing by this technique *metallic* from *semiconducting* silicides. In order to illustrate graphically the aforementioned difficulty, we reproduce in Fig. 2 the XPS valence-band spectra of Fe and β-$FeSi_2$ taken from Ref. 25 together with typical UPS spectra for Fe and β-$FeSi_2$ recorded in our conditions.

A detailed comparison between the measured DOS for the valence bands of β-$FeSi_2$ and FeSi and theoretical calculations[27] is shown in Fig. 3. The theoretical DOS has been obtained from an *ab initio* band-structure calculation performed within the local-density approximation, using the linear muffin-tin orbital method to solve self-consistently the one-electron wave equation. The calculation predicts β-$FeSi_2$ to be semiconducting with a band gap of 0.8 eV, in excellent agreement with our data and optical measurements of the band gap.[18–20] Furthermore, the figure reveals a nice correspondence between the experimental features observed at 0.8, 1.3, and 1.6 eV below E_F and the three peaks predicted to appear in this energy range by Christensen.[27] These peaks are related to nonbonding Fe 3*d* states,[27] and are enhanced in the experiment due to the larger cross sections of Fe 3*d* states vs Si 3*p* states at this photon energy. Between 2.5 and 3.5 eV, the Si 3*p*–Fe 3*d* bonding states are predicted in the calculations. They are hardly detectable in the experiment. The antibonding states are located *above* E_F.

We compare in Fig. 3 the FeSi UPS spectrum to the DOS of MnSi calculated self-consistently by the augmented-plane-wave method,[30] since to our knowledge no calculation of the DOS of FeSi itself exists. With the crystalline structure of both silicides being the same (cubic B-20), one can roughly reproduce the FeSi DOS by shifting the Fermi energy of MnSi, in order to account for the different number of electrons in the unit cell. We placed the Fermi energy at 13.2 eV, following Ref. 30. We have convoluted the theoretical DOS with a Gaussian of 0.1 eV full width at half maximum to account for the experimental broadening. The agreement is reasonable. The peak at 0.55 eV below E_F is assigned to nonbonding Fe 3*d* states. They are closer to E_F than for β-$FeSi_2$, following the general trend for chemical bonding in silicides [increasing the metal content moves the states derived from the *d* band of the metal towards E_F (Ref. 1)]. In particular, both theory and experiment give high DOS at E_F, confirming the metallic character of FeSi. The separation in energy between the peaks at 0.55 and 1.8 eV is smaller in FeSi than in the calculation for MnSi. This is probably due to a larger localization of Fe 3*d* electrons as compared to Mn 3*d* (due to the increase in number of electrons) resulting in a smaller hybridization and narrower bands. The higher DOS at E_F of FeSi vs β-$FeSi_2$ is clearly evidenced in Fig. 3.

B. Growth of Fe on Si(100)2×1

The mode of growth of Fe on Si(100)2×1 and the coverage calibration were determined by monitoring with

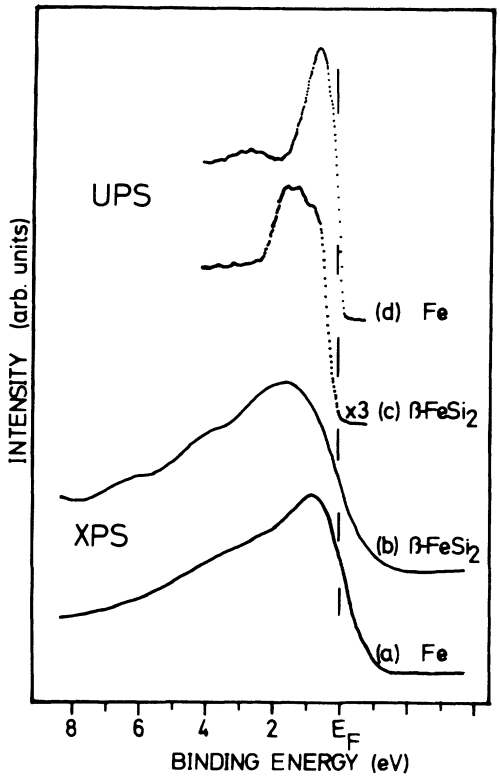

FIG. 2. Valence-band spectra for metallic Fe: (a) taken with XPS, and (d) taken with UPS. Valence-band spectra for thick films of β-$FeSi_2$: (b) taken with XPS, and (c) taken with UPS. Spectra (a) and (b) have been reproduced from Ref. 25 and illustrate the difficulty of detecting a semiconducting behavior with the limited resolution of unmonochromatized XPS.

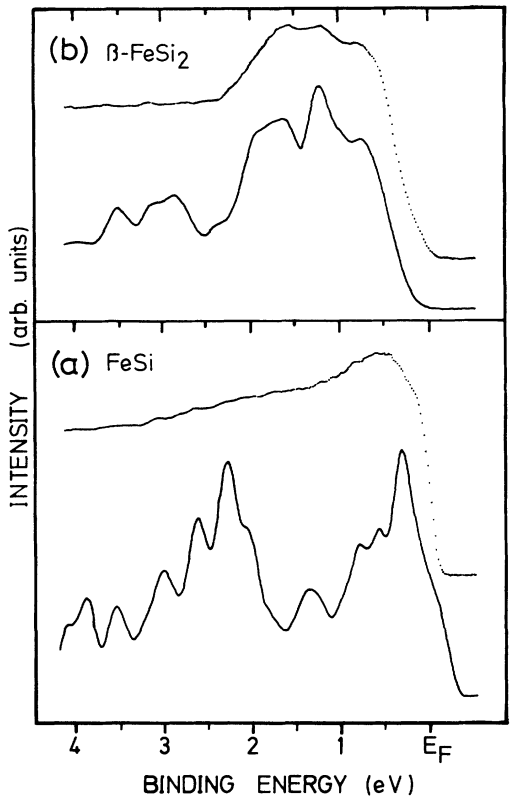

FIG. 3. (a) Comparison between the UPS spectrum (data points) for FeSi grown on Si(100) and the theoretical density of states (continuous line) of MnSi (Ref. 30). (b) Comparison between the valence-band spectrum for a β-$FeSi_2$ film grown on Si(100), represented by the data points and the theoretical density of states (continuous line) of Ref. 27. The experiments sample predominantly states of *d* character related to Fe, because of the difference in photoionization cross sections.

XPS the Fe $2p$ and Si $2p$ signals during the Fe deposition process. The Si $2p$ signal $I(\mathrm{Si}\ 2p)$ is exponentially attenuated when plotted versus the evaporation time, as evidenced by the linear behavior in logarithmic scale [Fig. 4(b)]. Since the thickness d of the Fe grown is proportional to the evaporation time t (assuming a constant sticking coefficient), this linear dependence of $I(\mathrm{Si}\ 2p)$ on t indicates that $I(\mathrm{Si}\ 2p)$ decays as

$$I(\mathrm{Si}\,2p)=I_{\mathrm{Si}}^{\infty}(e^{-d/\lambda_{\mathrm{Fe}}(1150)}) , \tag{3}$$

where I_{Si}^{∞} is the signal of a bulk, clean Si sample and $\lambda_{\mathrm{Fe}}(1150)$ is the IMFP of Si $2p$ photoelectrons (1150 eV kinetic energy) escaping through the Fe overlayer. The uniform attenuation shown in the plot indicates that the growth mode is layer-by-layer within XPS sensitivity. Nevertheless, further evidence provided by AES experiments[12,15] suggests that a small amount of Si could be dissolved in the Fe film (see also Sec. III C).

In a similar way the Fe $2p$ signal $[I(\mathrm{Fe}\ 2p)]$ follows the equation

$$I(\mathrm{Fe}\,2p)=I_{\mathrm{Fe}}^{\infty}(1-e^{-d/\lambda_{\mathrm{Fe}}(540)}) , \tag{4}$$

where I_{Fe}^{∞} is the signal of a bulk Fe sample and $\lambda_{\mathrm{Fe}}(540)$ is the IMFP of Fe $2p$ photoelectrons (540 eV kinetic energy) escaping through the Fe overlayer. The corresponding experimental points appear in Fig. 4(a).

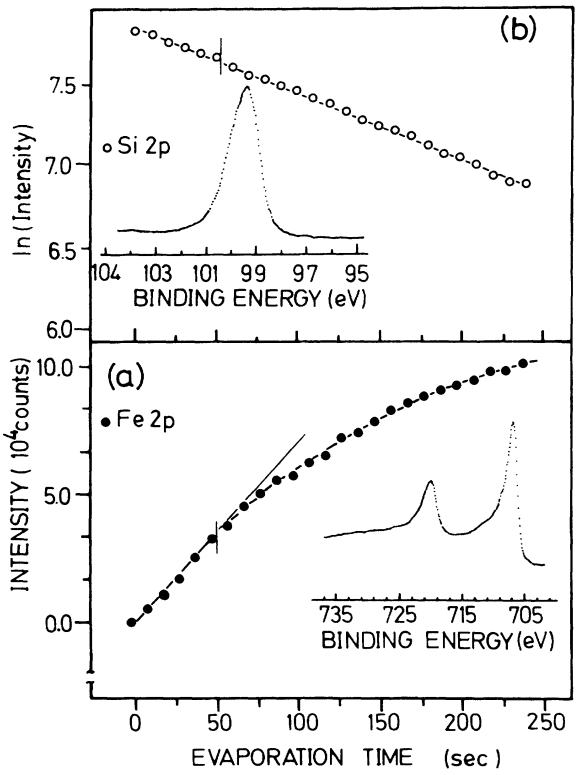

FIG. 4. Evolution of Fe $2p$ and Si $2p$ intensities during the growth of Fe on Si(100)2×1 at room temperature: (a) Fe $2p$ signal vs evaporation time. A break in the slope corresponding to the completion of the first monolayer is distinguished at ~50 s. The continuous line is a fit to the data yielding the IMFP of photoelectrons (see text). A typical Fe $2p$ spectrum is also displayed. (b) Attenuation of the Si $2p$ intensity (in logarithmic scale) vs Fe evaporation time. A typical Si $2p$ spectrum is displayed.

In order to fix the value of the horizontal scale of Fig. 4 in units of Å or monolayers (ML's), a value for the mean free paths or a calibration point is needed. From the experiment, [using Eqs. (3) and (4)], the ratio between both IMFP's can be directly calculated. We get a value $\lambda_{\mathrm{Fe}}(1150)/\lambda_{\mathrm{Fe}}(540)=0.67\pm0.2$. This ratio can be compared to the one obtained from the theoretical IMFP's of Ref. 31 [$\lambda_{\mathrm{Fe}}(1150)=13.4$ Å and $\lambda_{\mathrm{Fe}}(540)=7.8$ Å], which provide a ratio of 0.58, slightly smaller than the experimental one. These theoretical values can in principle be used to fix the horizontal scale of Fig. 4 in Å. We note that a closer inspection of the Fe $2p$ signal reveals that the data points can be fitted to a straight line up to ~50 s evaporation time. Assuming that the Fe coverage (θ) at this "break" point is low enough so that there is no attenuation of the Fe signal $[I(\mathrm{Fe}\ 2p)(\theta)]$, we get the value of the coverage by comparing this signal with the signal of the bulk, clean Si sample, I_{Si}^{∞}, since

$$I(\mathrm{Fe}\,2p)(\theta)=C\sigma_{\mathrm{Fe}}\theta \tag{5}$$

and

$$I_{\mathrm{Si}}^{\infty}=C\sigma_{\mathrm{Si}}\rho^{\mathrm{Si}}\lambda_{\mathrm{Si}}(1150) , \tag{6}$$

where σ_{Fe} (σ_{Si}) are the cross sections of Fe $2p$ (Si $2p$) for photons of 1253.6 eV, and include the energy dependence of the analyzer transmission function at constant pass energy $[I(E)\sim 1/E]$; ρ^{Si} is the atomic density of silicon; $\lambda_{\mathrm{Si}}(1150)$ is the IMFP of Si $2p$ photoelectrons escaping through Si, which we take equal to 23.0 Å, in agreement with the literature[33] and our own measurements;[32] and C is a constant which depends only on the x-ray flux and geometrical aspects of the detection process.

In short, we get that

$$\theta=\frac{I(\mathrm{Fe}\,2p)(\theta)}{I_{\mathrm{Si}}^{\infty}}\frac{\sigma_{\mathrm{Si}}}{\sigma_{\mathrm{Fe}}}\rho^{\mathrm{Si}}\lambda_{\mathrm{Si}}(1150) . \tag{7}$$

Applying this equation at the observed break, we get $\theta=(1.8\pm0.2)\times10^{15}$ atoms/cm^2. This value is very close to the atomic density of a [110] layer of bcc Fe (1.7×10^{15} atoms/cm^2). Therefore we assign this break to completion of the first Fe layer. As a check of consistency, we note that using the previously cited theoretical IMFP for Fe $2p$ photoelectrons [$\lambda_{\mathrm{Fe}}(540)=7.8$ Å] and Eq. (4), we can calculate the mean thickness corresponding to the break. The experimental $d/\lambda_{\mathrm{Fe}}(540)$ ratio at the break is 0.272, giving a mean thickness of 2.12 Å, equal within a 10% accuracy to the [110] interlayer distance for bcc Fe (2.03 Å).

In conclusion, we attribute the break at ~50 s to the completion of the first Fe monolayer. This assignment fixes the horizontal scale of Fig. 4 in ML, and determines the experimental values for $\lambda_{\mathrm{Fe}}(540)$ and $\lambda_{\mathrm{Fe}}(1150)$ as 7.2 and 10.5 Å. The error of these values is about 15%. They compare well with the theoretically calculated IMFP,[31] and provide us with a thickness scale in Å.

C. Evolution of the electronic structure during the Fe growth

The valence band corresponding to the growth of Fe on Si(100)2×1 at RT is shown in Fig. 5 for amounts of Fe ranging from 0.0 up to 1 ML, and in Fig. 6 for Fe coverages from 1.0 up to 5.5 ML. For clean Si(100)2×1 the Fermi level is 0.4 eV above the valence-band edge and the surface states, 0.7 eV above the valence-band edge. The characteristic structured peak (at our detection angle) due to the dangling-bond derived surface states is well resolved. The deposition of 0.06 ML of Fe slightly increases the emission at ~1 eV binding energy and shifts the valence-band edge by 0.3 eV towards the Fermi level. Higher coverages progressively deplete the Si derived states at ~2.2 eV, while the Fe *d* states give rise to the increase in intensity below ~0.5 eV. Surface metallization is achieved at ~1 ML coverage as evidenced by the appearance of emission at the Fermi energy (4–5 times less intense than for metallic Fe). Further Fe deposition (Fig. 6) moves the *d*-derived features closer to the Fermi level. Increasing the Fe coverage to 2 ML produces the appearance of a set of features at 0.5, 1.3, and 2.6 eV different from those observed below and above. On the basis of the calculated DOS for Fe_3Si,[22] they may be ascribed to direct formation of Fe_3Si. This is supported by a quantitative evaluation of the evolution of the surface-sensitive Auger peaks of Fe and Si during evaporation at RT.[15] It has been proposed that for a critical metallic coverage spontaneous formation of glassy silicidelike compounds takes place.[34] This would be observed here for Fe deposition at RT on Si(100) at coverages between 2 and 3 ML. Further increase in the Fe coverage produces peaks at 1 eV and ~2.6 eV, as unreacted, metallic Fe begins to form. The line shape of the valence band of bulk metallic Fe is only reached at $\theta_{Fe} > 5$ ML. At these coverages the UPS spectra agree well with previously published results for the valence band of Fe.[35]

D. Growth of iron silicides by SPE

We have studied the formation of iron silicides by SPE, a process consisting in the deposition of an Fe film onto the Si substrate (at RT), followed by sequential annealing to increasingly higher temperatures until a silicide film is formed. Figure 7(a) shows the $I(\text{Fe } 3p)/I(\text{Si } 2p)$ XPS intensity ratio plotted versus the annealing temperature for different initial Fe coverages. The coverage (θ) is measured in units of the atomic density of the [110] layer of bcc Fe (1.7×10^{15} atoms/cm^2). We performed a series of experiments for initial θ_{Fe} high enough to completely attenuate the Si signal below our detection level (an Fe coverage which we estimate over 20 ML). Under these conditions, the sampling depth can safely be assumed to surpass the thickness of the reacted layer, and the $I(\text{Fe } 3p)/I(\text{Si } 2p)$ intensity ratio provides a direct measurement of the atomic stoichiometry of the film. We note that for Fe coverages larger than 10 ML, the $I(\text{Fe } 3p)/I(\text{Si } 2p)$ intensity ratio remains constant in two different temperature ranges: from 400 °C up to

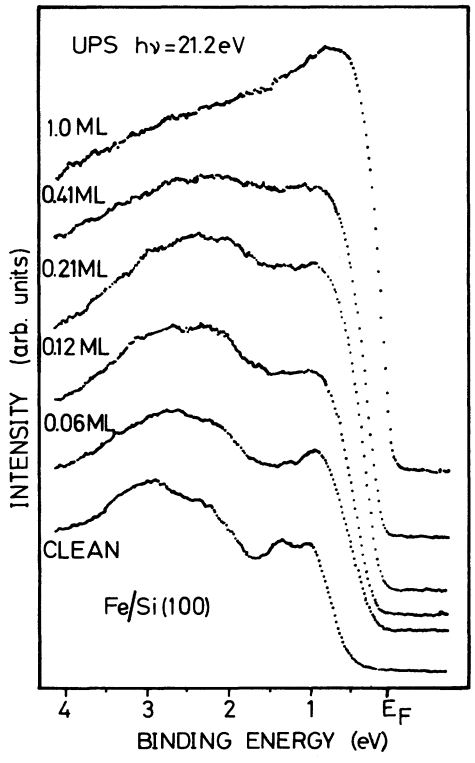

FIG. 5. Angle-integrated UPS spectra as a function of Fe coverage on Si(100) for $0.0 \le \theta_{Fe} \le 1.0$ ML. Note the progressive increase of the Fe-derived *d*-band intensity close to the Fermi energy.

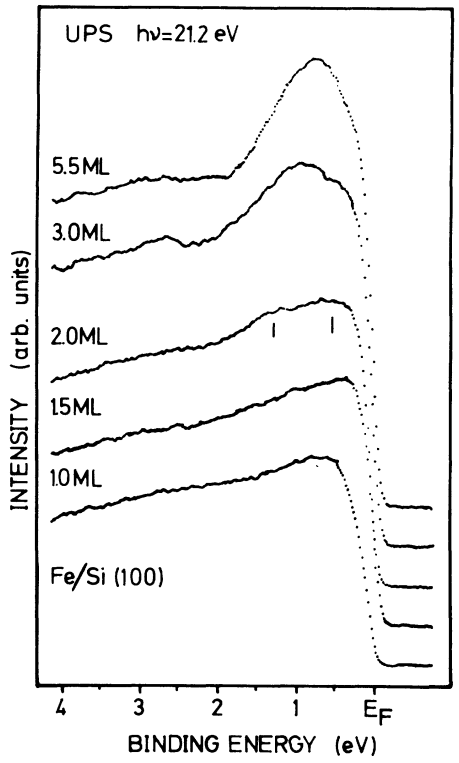

FIG. 6. UPS spectra of the valence band as a function of Fe coverage on Si(100) for $1.0 \le \theta_{Fe} \le 5.5$ ML. The last spectrum is identical to the one obtained for a thick Fe film.

570 °C, and from 600 °C up to 850 °C. The exact location and width of these plateaus depends on the actual value of the Fe coverage. The well-defined temperatures of appearance of these regions indicate that thermally promoted reactions have taken place, i.e., compounds of well-defined, bulklike stoichiometry have been formed.

In addition, the evolution of the energy loss for the Fe *LVV* Auger transition when performing a representative SPE process is displayed in Fig. 7(b). There is a clear change from a value of 22.0 eV (typical of FeSi) to a value of 20.7 eV (typical of β-$FeSi_2$). Furthermore, there are plateaus in the value of the energy loss correlated with the ones observed in the XPS ratios. This evidence supports the fact that the first plateau of the SPE experiments corresponds to FeSi, while the second one has the characteristic stoichiometry of $FeSi_2$. The transition from FeSi to $FeSi_2$ is rather sharp. The plateau for FeSi is seen for most Fe coverages. Only at the lowest one (2.5 ML) the I(Fe 3p)/I(Si 2p) ratio decays steadily. The plateau assigned to $FeSi_2$, however, is only seen at large coverage. Notice that in all cases, at temperatures above ~900 °C there is a further drop of the I(Fe 3p)/I(Si 2p) ratio to values around 0.1.

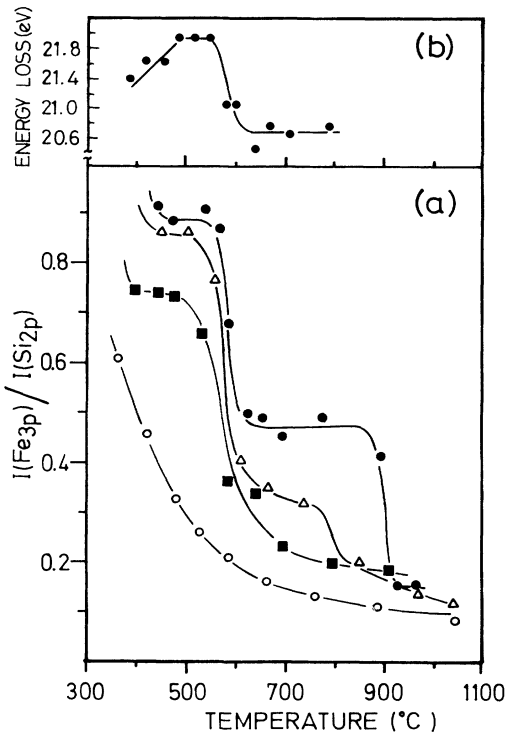

FIG. 7. (a) Evolution of the intensity ratio I(Fe 3p)/I(Si 2p) vs the annealing temperature for different initial Fe coverages deposited at room temperatures on Si(100). Symbols refer to the Fe coverage: solid circles (20 ML), open triangle (10 ML), solid squares (5.5 ML), and open circles (2.5 ML). The observed plateaus correspond to compounds of well-defined bulklike composition. (b) Plasmon energy loss at the Fe *LVV* peak excited with Mg $K\alpha$ photons vs annealing temperature for an initial Fe coverage of 20 ML. Note the appearance of two plateaus which agree well with those of panel (a).

E. Evolution of the electronic structure during the silicide formation

Selected UPS spectra taken during SPE of 20 ML of Fe are reproduced in Fig. 8. They are representative of the sequence of events that occurs during annealing of Fe films thicker than ~5 ML. In this range of Fe coverages, FeSi is the first silicide formed. The characteristic UPS spectrum of FeSi, with peaks at 0.55 and 1.8–2.0 eV and a decrease of the emission at E_F by a factor of ~3 with respect to metallic Fe, is first detected after annealing to 410 °C (in the first plateau of Fig. 7). From 650 °C to 875 °C, i.e., in the second plateau, β-$FeSi_2$ with its characteristic three peaks is formed. The emission at E_F falls by a factor 4–5 with respect to FeSi clearly indicating the semiconducting nature of β-$FeSi_2$. Furthermore, the Fermi level is pinned to the valence-band edge as expected for a p-doped degenerate semiconductor. In fact, transport measurements of thick, polycrystalline films of β-$FeSi_2$ have shown that, as grown, the material is heavily p doped with a density of carriers (~10^{19} cm^{-3}) dictated by the defect density.[20]

Increasing the temperature to 975 °C (i.e., in the drop from the second plateau of Fig. 7) produces a Si enrichment at the surface as detected by energy loss spectroscopy (ELS) and AES.[15] The corresponding valence-band spectra show a "high-temperature" phase characterized by a peak at 0.8 eV below E_F, a broad structure at ~3 eV, and weak emission (defect-related) at E_F. We identify this phase as a highly defected overlayer of outdiffused

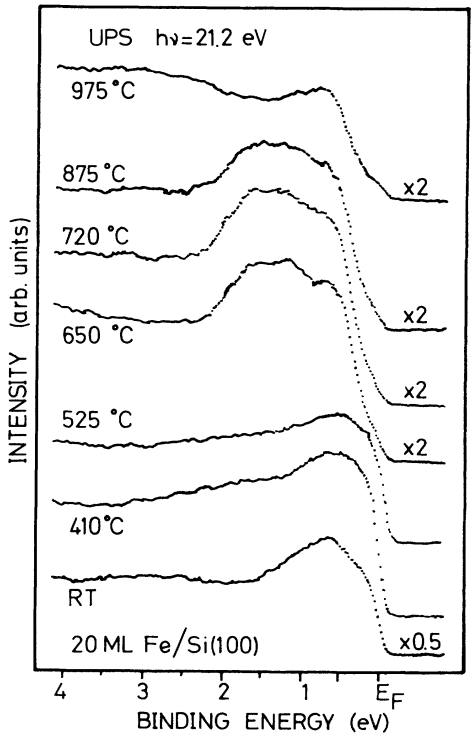

FIG. 8. Angle-integrated UPS spectra during the annealing of 20 ML of Fe deposited at room temperature (RT) on Si(100). The spectrum was recorded at RT after heating the sample 5 min to each temperature.

Si, the layer density of defects (dislocations) being responsible for the emission at E_F.

The valence-band spectra recorded during the process of SPE with 2.5 ML of Fe are reproduced in Fig. 9. The evolution is now different from the sequence of events described above for larger Fe coverages. In spite of the fact that no plateaus are seen in the $I(\text{Fe } 3p)/I(\text{Si } 2p)$ ratio, well-defined silicides are sequentially produced. As deposited, the spectrum shows peaks at 0.5, 1.3, and 2.6 eV and a metallic Fermi edge, indicating the formation of Fe_3Si directly at room temperature when depositing 2–3 ML of Fe (see also Sec. III C and Fig. 6). Annealing to 360 °C promotes the formation of FeSi with a prominent peak at 0.5 eV and almost no change in the DOS at E_F. At 420 °C an interesting change is observed: the spectrum displays peaks at 0.8 and 1.8 eV and emission at E_F. In spite of the fact that the composition of the overlayer, as judged from AES,[12] is $FeSi_2$, the spectrum is quite different from the one characteristic of β-$FeSi_2$. In particular, the metallic character of this compound has been reproducibly observed. The measured DOS compares well with the one calculated by Christensen for a hypothetical metallic phase of $FeSi_2$ with the fluorite structure.[27] In fact, such a fluorite phase of $FeSi_2$ has been stabilized on Si(111) by Onda *et al.*[28] They reported conditions for growing this phase (evaporation of 2–3 ML of Fe at RT and annealing to 450 °C for 5 min) almost identical to the ones used here. We do not know yet whether such a fluorite structure can also be stabilized on Si(100) surface, but structural studies are in progress to address this issue. In any case, the range of stability of this metallic phase is fairly small, since annealing to 530 °C results in a UPS spectrum displaying semiconducting behavior.

The outdiffusion of Si is detected at lower temperatures than before, in such a way that at 760 °C the UPS spectrum already corresponds to the "high-temperature" phase. There is evidence from LEED, which shows a 2×1 pattern from clean Si(100),[15] scanning tunnel microscopy (STM),[36] and ELS, which displays plasma losses from bulk Si (Ref. 12) that for these low Fe coverages annealed to high temperatures, the silicide film is not continuous, but it is rather in the form of small islands separated by patches of bare Si.

F. Growth of silicides by RDE

We performed a series of reactive-deposition epitaxy experiments in order to characterize the type and quality of the silicide films thus grown. In these experiments Fe is evaporated onto the Si substrate, which is maintained at a constant (and usually high) temperature. This enhances the diffusion of Si atoms under a constant flux of incoming Fe atoms, and facilitates the reaction. The various silicides can be prepared by RDE at the respective temperatures of formation. Figure 10 shows selected results from RDE at 475 °C. The inset depicts the evolution of the $I(\text{Fe } 3p)/I(\text{Si } 2p)$ intensity ratio versus

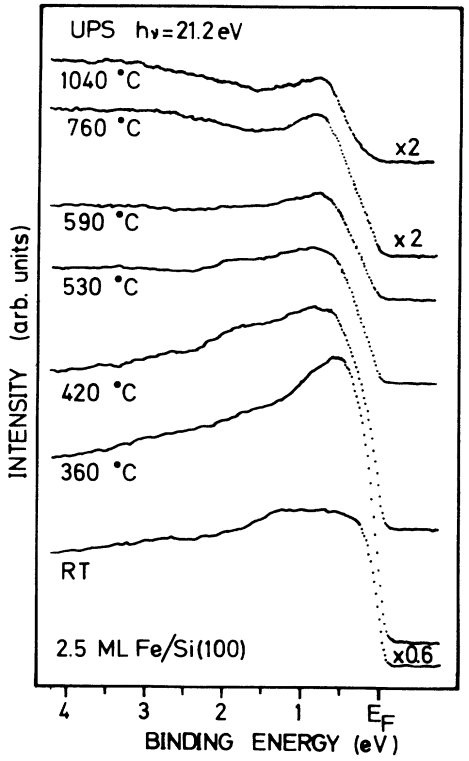

FIG. 9. Angle-integrated UPS spectra during the annealing of 2.5 ML of Fe deposited at room temperature (RT) on Si(100). The spectrum was recorded at RT after heating the sample 5 min to each temperature.

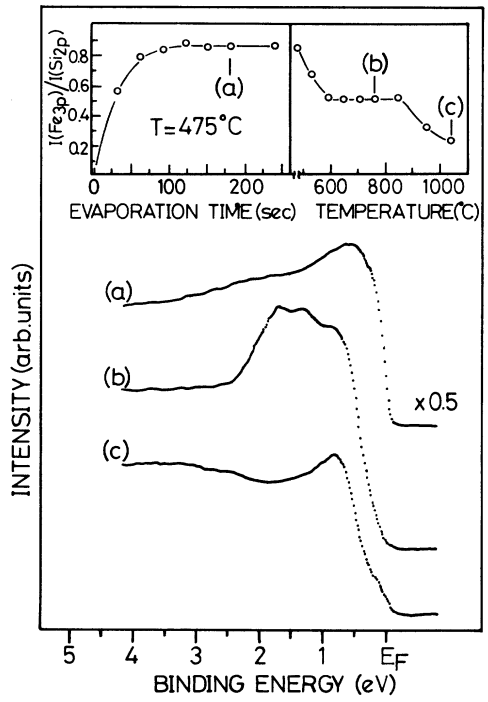

FIG. 10. The insets depict the evolution of the $I(\text{Fe } 2p)/I(\text{Si } 2p)$ vs Fe deposition time at 475 °C (i.e., at the first plateau of Fig. 8) and after annealing without further Fe evaporation. The UPS spectra (a), (b), and (c) have been taken at the points indicated in the insets. They correspond, respectively, to FeSi, β-$FeSi_2$, and the high-temperature phase.

evaporation time when the sample is kept at 475 °C, i.e., the temperature of the first plateau. The ratio reaches rather quickly a constant level, equal to the value for FeSi. The corresponding UPS spectrum [see Fig. 10(a)] shows in fact the line shape of metallic FeSi. Continuing the deposition at 475 °C produces no change in core-level ratio or valence-band spectra. Subsequent stepwise annealing of the films produces a plateau at the composition of β-$FeSi_2$. The UPS spectrum reveals the presence of three peaks at 0.8, 1.3, and 1.6 eV, the characteristic structure of β-$FeSi_2$. The Fermi level is close to the valence-band edge. The spectra obtained during this process have sharp, well-defined features and very low emission at E_F. This indicates a low density of defects and a higher quality of the epitaxial film than in the SPE case. At $T > 900$ °C, the $I(\text{Fe } 3p)/I(\text{Si } 2p)$ ratio drops and the valence band is identical to the final stage of the SPE process (see Figs. 8 and 9).

IV. CONCLUSIONS

A summary of our results is presented in Fig. 11 in the form of a coverage-temperature phase diagram showing the range of existence of the different iron silicides grown on Si(100). Vertical lines indicate SPE processes at fixed initial Fe coverage. Horizontal lines represent RDE processes at fixed substrate temperatures. As we have shown, by choosing the appropriate growth parameters any desired iron silicide can be selected and stabilized. Work is in progress to characterize in depth the phases that do not exist in the bulk Fe-Si phase diagram.

The growth of iron silicides on Si(100) has been examined by photoelectron spectroscopies. The electronic structure, the characteristic plasmon losses, and the atomic stoichiometry were determined for all observed phases, and the results were compared to bulk single crystals of FeSi(100) and α-$FeSi_{2.3}$(100). We have characterized the density of states of β-$FeSi_2$, FeSi, and Fe_3Si, and the experimental conditions which favor the growth of each phase. β-$FeSi_2$ is clearly semiconducting displaying a broad multipeak structure close to the Fermi energy. Each silicide presents a certain stability range (upon changing both the Fe amount and the annealing temperature), and the coexistence region is rather narrow. Both SPE and RED processes were employed to grow the silicide films. RDE allows one to grow thick, high quality β-$FeSi_2$ films more easily than SPE.

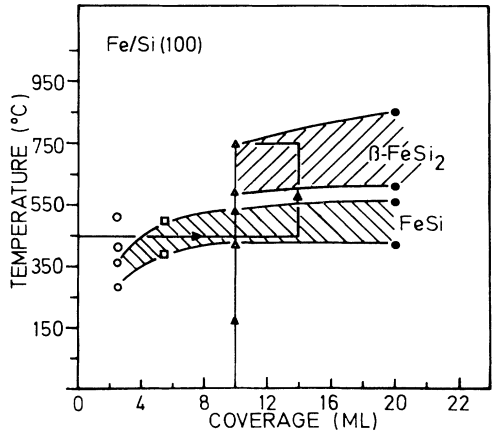

FIG. 11. Temperature-coverage phase diagram for the Fe/Si(100) system. The symbols (circles, squares, and triangles) correspond to SPE processes (described in the text) performed at different initial Fe coverages. Each SPE process corresponds to a vertical line. For the sake of clarity, only the one corresponding to 10 ML is shown. The horizontal solid line illustrates a process of RDE at 450 °C, followed by annealing to 750 °C (connecting vertical line) in order to reach the region of stability of β-$FeSi_2$. The regions of stability of several iron silicides are shown in the figure.

ACKNOWLEDGMENTS

We thank C. Limones for helping us during some experiments. This work was supported by ESPRIT BRA No. P3026 and by the CICYT, and by Accion Integrada No. HA-059.

*Permanent address: Institut für Physikalische und Theoretische Chemie der Universität Bonn, Wegelerstrasse 12, 5300 Bonn 1, Germany.

[1]C. Calandra, O. Bisi, and G. Ottaviani, Surf. Sci. Rep. **4**, 271 (1981).
[2]P. S. Murarka, J. Vac. Sci. Technol. **17**, 775 (1980).
[3]N. Cherief, R. Cinti, M. de Crescenzi, J. Derrien, T. A. Nguyen Tan, and J. Y. Veuillen, Appl. Surf. Sci. **41/42**, 241 (1989).
[4]R. T. Tung, J. Vac. Sci. Technol. A **7**, 598 (1989).
[5]L. J. Brillson, Surf. Sci. Rep. **2**, 123 (1982).
[6]P. Y. Dusasoy, J. Protas, R. Wandji, and B. Roques, Acta Crystallogr. Sec. B **27**, 1209 (1971).
[7]R. Bucksch, Z. Naturforsch A **22**, 2124 (1967).
[8]U. Birkholz and J. Schelm, Phys. Status Solidi **27**, 413 (1968); **34**, K177 (1969).
[9]I. Nishida, Phys. Rev. B **7**, 2710 (1973).
[10]B. Aronsson, T. Lundström, and S. Rundqvist, *Borides, Silicides and Phosphides* (Wiley, New York, 1965).
[11]J. E. Mahan, K. M. Geib, G. Y. Robinson, R. G. Long, Y. Xinghua, G. Bai, M-A. Nicolet, and M. Nathan, Appl. Phys. Lett. **56**, 2126 (1990).
[12]J. M. Gallego and R. Miranda, J. Appl. Phys. **69**, 1377 (1991).
[13]J. Alvarez, J. J. Hinarejos, E. G. Michel, J. M. Gallego, A. L. Vázquez de Parga, J. de la Figuera, C. Ocal, and R. Miranda, Appl. Phys. Lett. **59**, 99 (1991).
[14]S. Kennou, N. Cherief, R. R. Cinti, T. A. Nguyen Tan, and J. Y. Veuillen, Surf. Sci. **211/212**, 685 (1989).
[15]J. M. Gallego, Ph.D. thesis, Autonomous University of Madrid, 1991.
[16]T. Hirano and M. Kaise, J. Appl. Phys. **68**, 627 (1990).
[17]F. A. Sidorenko, P. V. Geld, and L. B. Dubroskaya, Fiz. Met. Metalloved. **8**, 735 (1959).
[18]M. C. Bost and J. E. Mahan, J. Appl. Phys. **58**, 2696 (1985).
[19]K. Lefki, P. Muret, N. Cherief, and R. C. Cinti, J. Appl. Phys. **69**, 352 (1991).

[20]C. A. Dimitriadis, J. H. Werner, S. Logothetidis, M. Stutzmann, J. Weber, and R. Nesper, J. Appl. Phys. **68**, 1726 (1990).
[21]G. R. Castro and A. Ballesteros, Surf. Sci. **204**, 415 (1988); and (unpublished).
[22]J. Kudrnovsky, N. E. Christensen, and O. K. Andersen, Phys. Rev. B **43**, 5924 (1991).
[23]J. Alvarez, J. J. Hinarejos, E. G. Michel, J. M. Gallego, and R. Miranda, Surf. Sci. **251/252**, 59 (1991).
[24]B. Egert and G. Panzner, Phys. Rev. B **29**, 2091 (1984).
[25]M. De Crescenzi, G. Gaggiotti, N. Motta, F. Patella, A. Balzarotti, and J. Derrien, Phys. Rev. B **42**, 5871 (1990).
[26]Baoqui Li, Mingron Ji, and Jianxin Wu, J. Appl. Phys. **68**, 1099 (1990).
[27]N. E. Christensen, Phys. Rev. B **42**, 7148 (1990).
[28]N. Onda, J. Henz, E. Müller, K. A. Mäder, and H. von Känel, Appl. Surf. Sci. **56-58**, 421 (1992).
[29]C. J. Powell and M. P. Seah, J. Vac. Sci. Technol. A **8**, 735 (1990).
[30]O. Nakanishi, A. Yanase, and A. Hasegawa, J. Magn. Magn. Mater. **15-18**, 879 (1980).
[31]David R. Penn, J. Electron Spectrosc. Relat. Phenom. **9**, 29 (1976).
[32]E. G. Michel, Ph.D. thesis, Autonomous University of Madrid, 1988.
[33]M. F. Hochella and A. H. Carim, Surf. Sci. Lett. **197**, L260 (1988).
[34]A. Hiraki, Surf. Sci. Rep. **3**, 357 (1984).
[35]M. Pessa, P. Heimann, and H. Neddermeyer, Phys. Rev. B **14**, 3488 (1976).
[36]A. L. Vázquez de Parga, J. de la Figuera, C. Ocal, and R. Miranda, Ultramicroscopy (to be published).